

This document is confidential and is proprietary to the American Chemical Society and its authors. Do not copy or disclose without written permission. If you have received this item in error, notify the sender and delete all copies.

HMBVIP: A Novel Hierarchical Multi-Bio-View Intelligent Prediction Networks for Drug-target Interaction Prediction

Journal:	<i>Journal of Chemical Information and Modeling</i>
Manuscript ID	Draft
Manuscript Type:	Article
Date Submitted by the Author:	n/a
Complete List of Authors:	Yang, Hailong; Jiangnan University, School of Artificial Intelligence and Computer Science Ning, Qiao; Jiangnan University, School of Artificial Intelligence and Computer Science Song, Ze; Jiangnan University, School of Artificial Intelligence and Computer Science Chen, Yue; Jiangnan University, School of Artificial Intelligence and Computer Science Wang, Guanjin; Murdoch University, School of Information Technology Deng, Zhaohong; Jiangnan University, School of Artificial Intelligence and Computer Science Zuo, Yun; Jiangnan University, School of Artificial Intelligence and Computer Science Ge, Yuxi; Affiliated Hospital of Jiangnan University, Department of Radiology Hu, Sudong; Affiliated Hospital of Jiangnan University, Department of Radiology

SCHOLARONE™
Manuscripts

HMBVIP: A Novel Hierarchical Multi-Bio-View Intelligent Prediction Networks for Drug-target Interaction Prediction

Hailong Yang¹, Qiao Ning¹, Ze Song¹, Yue Chen¹, Guanjin Wang², Zhaohong Deng^{1,*}, Yun Zuo^{1,*}, Yuxi Ge^{3,*}, and Shudong Hu³

¹School of Artificial Intelligence and Computer Science, Jiangnan University, Wuxi 214122, China.

²School of Information Technology, Murdoch University, WA, 6150, Australia.

³Department of Radiology, Affiliated Hospital of Jiangnan University, Wuxi 214062, China.

*Corresponding Author: Zhaohong Deng(dengzhaohong@jiangnan.edu.cn); Yun Zuo(zuoyun@jiangnan.edu.cn); Yuxi Ge(gmy1986@126.com)

Abstract

Drug-Target Interaction (DTI) prediction plays a vital role in drug discovery. Recent advances in Artificial Intelligence (AI) have enabled automatic extraction of high-order features from biological data, reducing the need for manual feature engineering. While multi-view AI models improve prediction accuracy and robustness by integrating diverse data sources, they still face key limitations: (1) the use of single-scale sequence tokenizers which fail to capture biological information across multi granularities, and (2) shallow, single-layer view integration which overlooks the hierarchical biological relationships. To tackle these challenges, we propose the concept of “bio-token” and design a multi-scale biological tokenizer capable of preserving multi-resolution of biological features. We also introduce a novel Hierarchical Multi-Bio-View Learning (HMBV) approach, implemented in an end-to-end DTI prediction network termed HMBVIP. Our model combines the biological sequence view and graph view at the top level, while integrating the global evolutionary view with the local biochemical view at the second level. This hierarchical multi-view strategy enriches hidden representations with multi-dimensional biological context, thereby enhancing DTI prediction accuracy and biologically meaningful interpretation. Extensive experiments on benchmark datasets (DAVIS, KIBA and BindingDB) demonstrate that HMBVIP consistently outperforms current state-of-the-art models, highlighting its superior predictive capability.

Keywords: Bio-Token; Drug-Target Interaction (DTI); Drug Discovery; Multi-View Learning; Graph Attention;

1. Introduction

Drug-target Interaction (DTI) prediction plays a crucial role in the process of new drug discovery ^{1,2}. By utilizing biological and chemical data, it enables the rapid screening of compounds with high affinity for specific targets, thus significantly improving hit rates and substantially reducing experimental costs. Beyond primary screening, DTI prediction also assists in designing multi-target drugs for complex diseases, and supports drug repurposing effects by uncovering new therapeutic uses for existing compounds, saving time and resources ³. Moreover, it aids in the detection of potential off-target effects ^{4,5}, contributing to reduced drug side effects and enhanced drug safety. These capabilities make DTI prediction a valuable tool in advancing personalized medicine, and improving the precision and efficacy of drug interventions ^{6,7}.

Computational models for DTI have becoming popular for accelerating drug discovery and reducing development costs. Recent advances in machine learning have significantly contributed to the substantial progress in DTI prediction modelling ⁸. Notably, heterogeneous graph learning methods ⁹ and relation-aware transformers have been developed to model complex drug-target relationships through network integration ¹⁰.

However, these methods often fail to capture the hierarchical biological semantics inherent in biological data. The Kronecker Regularized Least Squares (KronRLS) method¹¹ integrates drug and target similarity matrices through Kronecker products, effectively capturing their interaction relationships and becoming a classic approach in this field. Subsequent improvements include SimBoost¹², which combines similarity analysis with boosting techniques to enhance predictive performance. DeepDTA¹³ shifts toward deep learning by employing convolutional neural networks (CNNs) to extract features directly from raw drug and target sequences. More recently, GraphDTA¹⁴ has advanced the field by representing molecules as graph structures and employing graph neural networks (GNNs) to capture intramolecular relationships.

Despite the progress in DTI prediction, several challenges remain. Firstly, the complexity of biological systems makes it difficult to reliably extract valuable information from complex biological data^{15–17}. For instance, identifying the importance of frequently occurring amino acid fragments in protein sequences is crucial. However, many prediction models^{18,19}, particularly those based on deep learning, exhibit limited biological interpretability. This limitation restricts researchers' ability to derive mechanistic understanding of drug-target interactions, thereby introducing uncertainty in high-stakes clinical applications²⁰. To address these issues, multi-view learning methods^{21–23} have also been introduced into DTI prediction. These models aim to mine deep data features and uncover hidden patterns by leveraging complementary data views, particularly under conditions of limited data^{24–26}. For example, Sheng et al. proposed the MccDTI²⁷ multi-view representation learning method, which integrates heterogeneous drug and target data to learn high-quality, low-dimensional representations. The method achieves it by integrating consistent and complementary information from multiple views. Similarly, the MINDG model²⁸ combines deep learning and graph learning to integrate higher-order graph information and structured sequential information to further improve the DTI prediction accuracy. Zeng et al. proposed the MvGraphDTA method²⁹, which extracts structural features from drug-target graphs, constructs edge-vertex relationships based on line graphs, and fuses the features from the multiple views. However, current multi-view DTI prediction methods mainly focus on data-centric views, and neglect biologically meaningful perspectives. As a result, these models struggle to identify biologically significant features critical to DTI mechanisms³⁰. In addition, these methods tend to obtain features from single-layer distant views, limiting their ability to capture hierarchical and multi-level nature of biological information³¹.

To address the aforementioned issues, we propose a novel Hierarchical Multiple Biological View (HMBV) learning method and develop an end-to-end prediction network, termed HMBVIP, as illustrated in Fig. 1. HMBVIP encompasses four biologically meaningful views: the global evolutionary view, local biochemical view, biological sequence (bio-sequence) view, and biological graph (bio-graph) view. By incorporating these diverse perspectives, the model embeds rich biological semantics into its hidden representations, enabling a deeper and more comprehensive understanding of drug-target interactions across multiple layers and dimensions. The main contributions of this work are summarized as follows:

- We introduce the concept of “biological token” (bio-token) and propose a multi-scale biological tokenizer that segments biological sequences at multiple levels of granularity. Guided by expert biological knowledge, this tokenizer generates token sequences enriched with biologically meaningful features, enhancing downstream model performance.

- We propose a hierarchical multi-bio-view learning method and design an end-to-end prediction network, namely HMBVIP. HMBVIP integrates diverse biological views in a layered structure, effectively capturing multi-dimensional and hierarchical biological relationships for improved DTI prediction.
- We conduct comprehensive evaluations of HMBVIP on both general DTI datasets and antiviral drug prediction tasks. Experimental results demonstrate that HMBVIP can accurately identify effective therapeutic compounds from known drug collections for specific viral diseases, significantly improving screening efficiency.

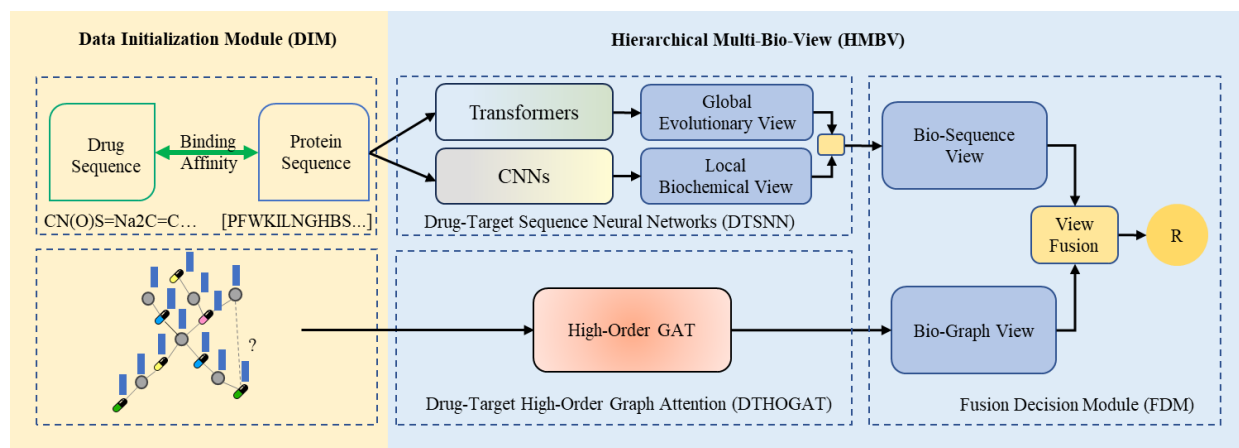


Figure 1. Structure of HMBVIP. The model comprises two core modules: 1) Data Initialization Module (DIM) processes drug and protein sequences, 2) Hierarchical Multi-Bio-View (HMBV) extracts drug-target features through multiple biological view, The HMBV module consists of three components: Drug-Target Sequence Neural Networks (DTSNN), Drug-Target High-Order Graph Attention (DTHOGAT), and Fusion Decision Module (FDM).

2. Materials and Methods

HMBVIP consists of two modules: the Data Initialization Module (DIM) and the Hierarchical Multi-Bio-View (HMBV) module. Within the HMBV module, three key components are integrated: Drug-Target Sequence Neural Networks (DTSNN), Drug-Target High-Order Graph Attention (DTHOGAT), and the Fusion Decision Module (FDM). This structure employs a hierarchical multi-bio-view learning strategy that operates across two distinct layers of biological views. The first layer within DTSNN incorporates the global evolutionary and the local biochemical views, while the second layer realized in FDM integrates the bio-sequence view and the bio-graph view. Through leveraging these hierarchically organized biological views, HMBVIP effectively uncovers latent patterns and interactions between drugs and targets, enriching the semantic depth of latent variables with biologically meaningful information. This strategy not only improves the accuracy of DTI but also enhances the model's biological interpretability. The overall architecture of HMBVIP is depicted in Fig. 1.

2.1 DTI Datasets

To evaluate the performance of HMBVIP, we used two widely used benchmark datasets: DAVIS, KIBA and BindingDB. The characteristics of each dataset are outlined below.

The DAVIS^{25,32} dataset includes clinically relevant kinase inhibitors and their dissociation constants (kinase dissociation constant K_d), encompassing 25,772 drug-target pairs, covering 68 drugs and 379 different target proteins. The connection label in the data is the K_d value. To enhance the stability of the training process, we adopted the method from Öztürk et al., converting the original K_d values into their logarithmic form pK_d , with the specific conversion as shown in Eq. (1).

$$pK_d = -\log_{10} \left(\frac{K_d}{1e9} \right) \quad (1)$$

where pK_d is the binding affinity between a drug and a target. A pK_d value of 7 or higher indicates a strong interaction between the drug and the target.

In the KIBA^{6,25} study, the dataset was integrated by combining IC₅₀, K_i , and K_d labels to enhance information complementary. This research focuses on a sub-dataset for in-depth analysis. The sub-dataset uses K_d values as the key labels and includes 117,657 drug-target pairs involving 2,068 different drugs and 229 target proteins. Based on Eq. (1), the K_d values are converted to pK_d values and set that a pK_d value of 12.1 or higher indicates a strong interaction between the drug and the target.

BindingDB³³ is a public, web-accessible database of measured binding affinities, focusing chiefly on the interactions of proteins considered to be candidate drug-targets with ligands that are small, drug-like molecules. As of March, 2011, BindingDB contains about 650,000 binding data, for 5,700 protein targets and 280,000 small molecules. BindingDB also includes a small collection of host-guest binding data of interest to chemists studying supramolecular systems.

A generalized description of the datasets used in the experiments is shown in Table 1.

Table 1 A Brief Description of The Datasets

Dataset	Drug/Target	DTI Pairs			
		Train (70%)	Valid (10%)	Test (20%)	Total
DAVIS	68/379	18040	2577	5154	25772
KIBA	2068/229	82360	11766	23541	117657
BindingDB	10665/1413	36599	5228	10457	52284

2.2 Data Initialization Module (DIM)

The Data Initialization Module (DIM) serves as the module for initializing multiple data. It comprises two primary components: the initialization of the sequence data detailed in Section 2.2.1 and the initialization of the graph data detailed in Section 2.2.2.

2.2.1 DTI Sequence Data Initialization Based on Bio-Tokenization

In the DTI dataset, drug sequences adhere to the SMILES coding convention for chemical symbol sequences^{34,35}. The target protein sequences consist of 20 known amino acids (A, R, N, D, C, Q, E, G, H, I, L, K, M, F, P, S, T, W, Y, V). These original drug sequences and protein target sequences can be directly obtained from the ‘Drug’ and ‘Target’ fields in samples from the DAVIS, KIBA and BindingDB datasets.

Before utilizing sequence data for modelling, effective tokenization is essential to preserve biological structure and meaning. Protein sequences can be naturally decomposed into fragments at multiple biological scales. Under the influence of environmental factors such as temperature and pH levels, proteins break down into polypeptides³⁶. These polypeptides typically consist of 10 to 100 amino acids and are referred to as long-chain peptides. These polypeptides can further degrade into oligopeptides or short peptides, which usually contain fewer than 10 amino acids, under the influence of hydrolysis reactions, physical methods, or environmental factors³⁷. The biological terms "protein", "polypeptide", "oligopeptide", and "amino acid" represent different scales of amino acid fragments in biological semantics^{38–40}.

Inspired by hierarchical structure of protein sequences, we introduce the concept of “biological token” (bio-token),

which integrates domain-specific biological knowledge with natural language-inspired tokenization strategies. Based on this concept, we develop Bio-Tokenizer, a multi-scale biological tokenizer designed to segment protein sequences into biologically meaningful fragments. Bio-Tokenizer automatically decomposes amino acid sequences into high-frequency polypeptide and oligopeptide fragments.

Drug molecules are composed of the atoms such as carbon, hydrogen, oxygen, nitrogen, sulfur, halogens, phosphorus, and metal elements. However, individual atoms cannot effectively characterize the functional semantics of drugs ^{41,42}. The functional groups in drug molecules are collections of atoms that impart specific chemical and biological properties. As a result, we decompose the drug sequences based on their functional groups, specifically involving hydroxyl (-OH), carboxyl (-COOH), keto (-C=O), aldehydes (-CHO), thiols (-SH), sulphur ethers (-S-), and together with the halogen atoms (-F, -Cl, -Br, -I), metal elements (Fe, Mg, Zn, Ca, etc.) ^{41,43}. The addition of these tokens, which represent the functional semantics of drugs, enhances the vocabulary. This enables Bio-Tokenizer to effectively segment drug sequences while preserving their functional semantics.

The proposed Bio-Tokenizer addresses fundamental limitations in conventional protein sequence processing by explicitly preserving evolutionarily conserved functional elements. While standard approaches tokenize protein sequences into individual amino acids, this granularity fails to capture biologically meaningful peptide motifs that frequently mediate molecular interactions. Our methodology combines evidence-based motif discovery with data-driven token optimization, first compiling validated functional segments from curated databases including Pfam ⁴⁴, ELM ⁴⁵, and UniProtKB/Swiss-Prot ⁴⁶. These biologically significant patterns (e.g., integrin-binding "RGD", SH3 domain-interacting "PxxP", and nucleotide-binding "GxGxxG" motifs) form the core vocabulary, which is subsequently expanded through Byte Pair Encoding (BPE) trained on the UniProtKB reference proteome (release 2023_03). This hybrid approach ensures coverage of both known functional elements and statistically prevalent sequence patterns, with vocabulary items constrained to biochemically plausible lengths (3-15 residues). The tokenizer dynamically weights motifs by their evolutionary conservation scores from InterPro, prioritizing high-confidence functional units during the segmentation process with the Bio-Tokenization algorithm, which is shown in Algorithm I.

Algorithm I: Bio-Tokenization

Input: sequence $\mathbf{src} = [b_1, b_2, \dots, b_L]$, L is the sequence length;

UniProtKB and PubChem raw sequences U_p

Motifs from Published Articles D_{motif}

Biological Vocabulary V_{bio}

BPE Vocabulary V_{bpe}

Motif max size k_{max}

Output: Tokenized Sequence \mathbf{tar}

Procedure:

1: $V_{bio} := \{m \mid m \in D_{motif} \text{ and } \text{len}(m) \leq k_{max}\}$

2: $V_{bpe} := \text{BpeTrainer}(U_p)$

3: $\mathbf{tar} := []$

4: $i := 1$

5: **while** $i \leq L$ **do**

6: **for** $l := \min(k_{max}, L - i + 1)$ **to** 1 **do**

7: **if** $\mathbf{src}[i:i+l-1] \in V_{bio}$ **then**

8: $\mathbf{tar.append}(S[i:i+l-1])$

9: $i := i + l$

10: **break**

11: **else if** $\mathbf{src}[i:i+l-1] \in V_{bpe}$ **then**

12: $\mathbf{tar.append}(\mathbf{src}[i:i+l-1])$

```

13:      $i := i + l$ 
14:     break
15:   else
16:      $\mathbf{tar}.append(\mathbf{src}[i])$ 
17:      $i := i + l$ 
18:   end if
19: end for
20: end while
21: return  $\mathbf{tar}$ 

```

The processing function of Bio-Tokenizer is shown in Eq. (2)-(3). The Bio-Tokenizer maximally retains the biological information of protein sequences and provides support for the biological interpretation of model decisions.

$$\mathbf{t} = \text{BioTokenizer}(\mathbf{s}_{\text{protein}}) \quad (2)$$

$$\mathbf{d} = \text{BioTokenizer}(\mathbf{s}_{\text{drug}}) \quad (3)$$

where $\mathbf{s}_{\text{protein}}$ is the amino acid sequence, \mathbf{t} is the peptide sequence that has been sliced by the Bio-Tokenizer, \mathbf{s}_{drug} is the SMILES sequence of the drug, \mathbf{d} is the sequence of the drug functional group that has been sliced by the Bio-Tokenizer.

2.2.2 DTI Graph Data Initialization

As direct association data between drugs and targets are typically unavailable, the drug-target graph should be inferred from known DTI datasets. To represent this graph, we construct adjacency matrices that encode the connectivity between drug and target nodes, enabling efficient structural analysis.

The process of constructing a drug-target graph involves three key steps: firstly, nodes are defined to represent individual drugs and targets; secondly, edges are introduced between nodes based on known interaction data, reflecting potential relationships, and finally, a complete drug-target graph is formed by connecting drug and target nodes through the defined edges. Various methods exist for encoding the features of drug and target nodes, such as one-hot encoding, BERT model encoding, PSSM feature encoding, and evolutionary encoding. In this study, one-hot encoding was employed to represent node features due to its straightforward implementation and ease of interpretation.

2.3 Hierarchical Multi-Bio-View (HMBV)

The Hierarchical Multi-Bio-View (HMBV) serves as the core component of HMBVIP, designed to learn interaction features through multiple perspectives of DTI data. It consists of three components: the Drug-Target Sequence Neural Networks (DTSNN), the Drug-Target High-Order Graph Attention (DTHOGAT), and the Fusion Decision Module (FDM).

2.3.1 Drug-Target Sequence Neural Networks (DTSNN)

DTI sequence data characterize the internal composition of drug and target with rich structural and biological semantic information. To deeply capture these biological semantic features, DTSNN ingeniously incorporates two unique biological views: the global evolutionary view and the local biochemical view, as shown in Fig. 2. Building upon the insights derived from these two perspectives, DTSNN ultimately generates the bio-sequence view (as illustrated in the right gray box of Fig.2).

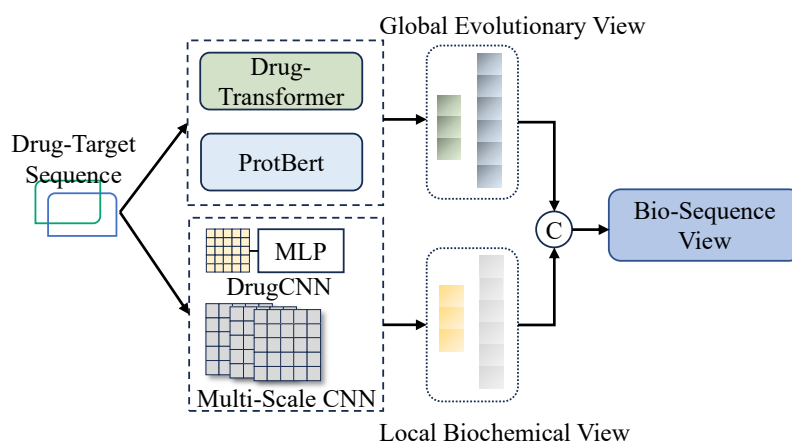


Figure 2. Structure of DTSNN. This module processes drug-target sequences through parallel pathways: 1) Global Evolutionary View (top branch) extracts high-level features via Drug-Transformer (drugs) and ProtBert (proteins), while 2) Local Biochemical View (bottom branch) captures local patterns using DrugCNN (single-scale) and Multi-Scale CNN (proteins). Features from both views are concatenated to construct the Bio-Sequence View.

Global Evolutionary View

To model drug-target interactions from the global evolutionary view (as illustrated in the top half of Fig. 2), we utilize two Transformer-based models equipped with multi-head attention mechanisms: Drug-Transformer and ProtBert models^{47,48}. These models are designed to capture long-range dependencies and global contextual information.

ProtBert is a pre-trained model designed by Elnaggar, specifically for extracting features of orthogonal protein sequences⁴⁹. Target proteins are synthesized from the transcription of DNA, which themselves characterize biological genetic information. ProtBert can capture the evolutionary information of a protein family, thereby extracting the evolutionary features of target proteins. Drug-Transformer is a drug sequences model based on the transformer architecture, aiming to reveal the deep features of drug chemical atoms, chemical bonds, and structures. When a drug has a strong affinity with the target protein, there exists a mapping relationship between the features of the drug and the target protein. Therefore, the drug can also indirectly characterize the evolution of the target protein family. Drug-Transformer obtains the global features of drugs through the global attention mechanism, while also indirectly extracting the evolutionary characteristics of the target protein. Finally, we connect the features of drugs and targets to obtain the global evolutionary features, as shown in Eq. (4).

$$Z_{global} = \text{Concat}(\mathcal{D}(\mathbf{d}), \mathcal{P}(\mathbf{t})) \quad (4)$$

where $\mathcal{D}(\cdot)$ is the unit processing function of Drug-Transformer, $\mathcal{P}(\cdot)$ is the unit processing function of ProtBert, Z_{global} is the latent features from the global evolutionary view, $Z_{global} \in \mathbb{R}^{1 \times d_g}$ and d_g is the global feature size, $d_g = d_d + d_t$, d_d is the drug feature size, d_t is the target protein feature size.

Local Biochemical View

For modelling drug-target interactions from the local biochemical view (as depicted in the bottom half of Fig. 2), we introduce two custom-designed models: DrugCNN and Multi-Scale CNN, aimed at capturing detailed local structural features of drugs and targets, respectively.

DrugCNN is developed to extract local connection patterns of chemical atoms and bonds within the molecules⁵⁰.

Compared with target proteins, the drugs have lower local structural complexity with lengths less than 100, DrugCNN is designed as a single-layer convolutional neural network (CNN), which is sufficient for capturing meaningful local structural representations. On the other hand, target protein sequence exhibit much longer sequences, potentially 20,000 amino acids, which is rich in biochemical information. To effectively capture the intricate local information, we design the Multi-Scale CNN, incorporating convolutional kernels of varying sizes to capture complex local information at different levels. This architecture allows the model to detect unique biochemical characteristics of the amino acid combinations at different scales. Ultimately, we integrate the features of drugs and targets to obtain a more comprehensive description of local biochemical features, as shown in Eq. (5).

$$\mathcal{Z}_{local} = \text{Concat}(\mathcal{C}_{ss}(\mathbf{d}), \mathcal{C}_{ms}(\mathbf{t})) \quad (5)$$

where $\mathcal{C}_{ss}(\cdot)$ is the unit processing function for the single kernel convolution and MLP of the drug sequence, d_s is the output feature size of $\mathcal{C}_{ss}(\cdot)$, $\mathcal{C}_{ms}(\cdot)$ is the unit processing function for the multi-scale multi-kernel convolutions of the target sequence, d_m is the output feature size of $\mathcal{C}_{ms}(\cdot)$, and \mathcal{Z}_{local} is the latent features from the local biochemical view, $\mathcal{Z}_{local} \in \mathbb{R}^{1 \times d_l}$ and d_l is the local feature size, $d_l = d_s + d_m$.

2.3.2 Drug-Target High-Order Graph Attention (DTHOGAT)

From a macroscopic perspective, DTIs encompass complex and structural biological relationships. These interactions can be modeled using the adjacency matrix, which captures pairwise associations and serves as the foundation for constructing a biological graph that integrates both protein family networks and drug-derived relationships.

We formally define the drug-target graph $G = (\mathcal{V}, \mathcal{E})$ as an undirected graph, $\mathcal{V} = \{v_d^1, \dots, v_d^\eta, v_t^1, \dots, v_t^\rho\}$, η is the total number of drug nodes, ρ is the total number of target protein nodes, $\mathcal{E} = \{(v_d^i, v_t^j), \dots, (v_d^i, v_t^j), \dots\}$, $i \in [1, \eta]$, $j \in [1, \rho]$. To effectively learn from this graph structure, we propose a novel drug-target graph network based on multilayer high-order graph attention networks (GAT)¹⁴, referred to as DTHOGAT (Fig. 3). DTHOGAT encodes the drug-target graph through multiple GAT layers and obtain high-order graph features, as shown in Eq. (6).

$$H^{(l)} = \parallel_{j \in P} \sigma(\hat{A}^j H^{(l-1)} W_j^{(l)}) \quad (6)$$

where $P = \{0, 1, 2, \dots, \zeta\}$ is the adjacency power, ζ is maximum of neighborhood of each GAT layer, \hat{A}^j is the adjacency matrix \hat{A} multiplied by j times, and \parallel denotes column-wise concatenation.

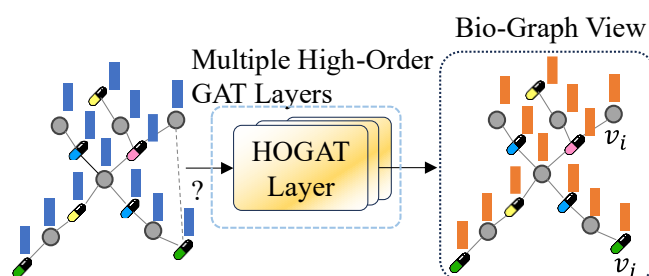


Figure 3. Structure of DTHOGAT. The model extracts drug-target graph features using multiple stacked High-Order Graph Attention (HOGAT) layers. In the illustrated graph, colored nodes represent entities (drugs as circles and targets as squares), while edges denote known interactions.

2.3.3 Fusion Decision Module (FDM)

To enable the integration of multi-perspective data, FDM conducts additional feature extraction on the bio-sequence

view derived from DTSNN and the bio-graph view generated by DTHOGAT, respectively.

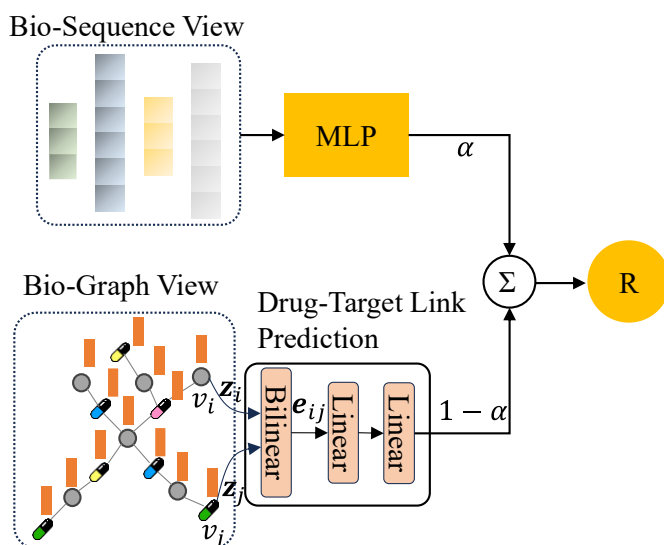


Figure 4. Structure of FDM, α is the views balance parameter, which is a learnable parameter for adaptively adjusting the weights of the two views: Bio-Sequence View and Bio-Graph View.

To further fuse both global and local information of the biological sequence, FDM extracts features from the bio-sequence perspective using a Multi-Layer Perceptron (MLP), as illustrated in Eq. (7).

$$\mathcal{R}_{seq} = \mathbf{W}_2 \left(\text{ReLU}(\mathbf{W}_1 [\mathcal{Z}_{global}; \mathcal{Z}_{local}] + \mathbf{b}_1) \right) + \mathbf{b}_2 \quad (7)$$

where \mathcal{R}_{seq} is the fusion result of the two views of DTSNN, and \mathcal{Z}_{global} and \mathcal{Z}_{local} are essentially intermediate hidden variables of the HMBVIP, \mathbf{W}_1 is the first layer weights of MLP, \mathbf{b}_1 is the first layer bias, \mathbf{W}_2 is the second layer weights, \mathbf{b}_2 is the second layer bias, $\mathbf{W}_1 \in \mathbb{R}^{(d_g+d_l) \times h}$, $\mathbf{W}_2 \in \mathbb{R}^{h \times d_{out}}$, h is the hidden size, d_{out} is the output feature size.

The link prediction module consists of a Bilinear network and two Linear networks. The Bilinear calculation is shown in Eq. (8). \mathcal{R}_{graph} is the result of drug-target link prediction in Eq. (9).

$$\mathbf{e}_{ij} = \text{ELU}(\mathbf{z}_i^T \mathbf{W}_b \mathbf{z}_j + b) \quad (8)$$

where \mathbf{z}_i and \mathbf{z}_j is the representations of node v_d^i and v_t^j , \mathbf{e}_{ij} is the edge representation, $\text{ELU}(\cdot)$ is exponential linear unit function.

$$\mathcal{R}_{graph} = \text{sigmoid} \left(\text{FC}_2 \left(\text{ELU} \left(\text{FC}_1(\mathbf{e}_{ij}) \right) \right) \right) \quad (9)$$

In the FDM module, we fuse the bio-sequence and bio-graph views using a weighted summation method, as illustrated in Fig. 4. The core idea of this method is to assign a tunable importance to each view. The weight of the bio-graph view is controlled by the balance coefficient α while the bio-sequence view is weighted by $1 - \alpha$, as illustrated in Eq. (10). To enable adaptive view fusion, α is set as a trainable parameter and is initialized at 0.8.

$$\mathcal{R} = \alpha * \mathcal{R}_{graph} + (1 - \alpha) * \mathcal{R}_{seq} \quad (10)$$

2.4 Hierarchical Multiple Biological View Learning

Hierarchical Multiple Biological View (HMBV) learning involves the joint training of multiple views. By accounting for the unique attributes of each view, we employ the cross-entropy loss function. To prevent overfitting, the HMBV incorporates an L2 regularization term, as illustrated in Equation (11).

$$\mathcal{L}_{HMBV}(\theta) = - \sum_{i=1}^n \mathcal{R} \log \hat{\mathcal{R}} + \gamma \|\theta\|_2 \quad (11)$$

where θ is the model parameters and γ is the influence factor of the L2 regular term, which takes the value of 0.01 in the experiments. The HMBV learning algorithm is shown in Algorithm 2.

Algorithm 2: HMBV Learning

Input: $s_{protein}$: target amino acid sequence; s_{drug} : drug SMILES raw sequence; E_p : maximal number of epochs;

Output: model parameters θ

Procedure:

```

1: for  $e = 1..E_p$  do
    // gain bio-token sequences of DTI
2:    $t = BioTokenizer(s_{protein})$ 
3:    $d = BioTokenizer(s_{drug})$ 
    // layer 1 views
4:   gain global evolutionary view  $Z_{global}$  as Eq. (4)
5:   gain local biochemical view  $Z_{local}$  as Eq. (5)
    // layer 2 views
6:   gain bio-sequence view through contacting  $[Z_{global}; Z_{local}]$ 
7:   gain bio-graph view  $G = (\mathcal{V}, \mathcal{E})$  as Eq. (6)
8:   predict the results  $\mathcal{R}_{seq}$  and  $\mathcal{R}_{graph}$  based on the views of step 6 and 7, as Eq. (7) and (9)
9:    $\mathcal{R} = \alpha * \mathcal{R}_{graph} + (1 - \alpha) * \mathcal{R}_{seq}$ 
10:   $\theta := \operatorname{argmin}_{\theta} \mathcal{L}_{HMBV}$ , minimize  $\mathcal{L}_{HMBV}$  as Eq. (11)
11: end for
12: return  $\theta$ 

```

3. Experiments

3.1 Metrics

The HMBVIP model is specifically designed for link prediction regression tasks, aiming to accurately predict the binding affinity values between nodes. To comprehensively evaluate the performance of this model, we adopted Mean Squared Error (MSE) and Concordance Index (CI) as key evaluation metrics.

The MSE is calculated by taking the average of the square of the difference between the true value \hat{y}_i and the predicted value y_j , with the specific formula shown in Eq. (12).

$$MSE = \frac{1}{n} \sum_{i=1}^n (\hat{y}_i - y_i)^2 \quad (12)$$

where n represents the number of drug-target pairs. And a lower MSE indicates superior performance in the link prediction.

The CI is a statistical measure that assesses the degree of concordance between the predicted binding affinity values of two drug target pairs and their true values as defined in Eq. (13).

$$CI = \frac{1}{N} \sum_{y_i > y_j} h(\hat{y}_i > \hat{y}_j)^2 \quad (13)$$

where \hat{y}_i is the predicted value of the larger affinity y_i , \hat{y}_j is the predicted value of the smaller affinity y_j , $h(\cdot)$ is a step function as defined in Eq. (14). A higher CI result indicates a more accurate prediction.

$$h(x) = \begin{cases} 1, & x > 0 \\ 0.5, & x = 0 \\ 0, & \text{else} \end{cases} \quad (14)$$

3.2 Baselines

To evaluate the effectiveness of HMBVIP, we conducted comparative experiments against six representative baseline methods: SimBoost¹², KronRLS⁵¹, DeepDTA¹³, GraphDTA¹⁴, MccDTI²⁷ and MvGraphDTA²⁹.

The key hyperparameters for the HMBVIP model are detailed in Table 2. During the training phase of HMBVIP, the configured parameters include an epoch count of 80, a batch size of 8, and a learning rate of 0.01.

Table 2 The Hyperparameters of HMBVIP

Module	Parameter	Value
DrugTransformer in DTSNN	n_layer	3
	n_head	16
	embedding_dim	128
DrugCNN in DTSNN	kernel size	3
	feature_in	32
	feature_out	128
Multi-Scale CNN in DTSNN	kernel size	{2,3,4,5}
	embedding_dim	128
	num feature_out	32
DTHOGAT	hidden_channels	4096
	out_channels	128

3.3 Prediction performances

We compared HMBVIP with the baseline methods using 10-fold cross-validation on the datasets. According to Table 3, HMBVIP achieved a 12.4% reduction in MSE compared to the best-performing baseline method, MvGraphDTA, while also improving the CI 0.7%. Further analysis of the data in Table 3 reveals that HMBVIP exhibits even more impressive performance, with an average MSE of only 0.007, lower than the optimal baseline method, GraphDTA, and a CI reaching 0.002, higher than that of GraphDTA. From Tables 3, the results demonstrate that HMBVIP outperforms other baselines, primarily due to the introduction of the HMBV learning method. The hierarchical multi-view learning paradigm of HMBV allows the model to deeply capture the latent representations within the data.

Table 3 Performance Comparison of Different Methods

Methods	DAVIS		KIBA		BindingDB	
	MSE↓	CI↑	MSE↓	CI↑	MSE↓	CI↑
KronRLS	0.379±0.004	0.871±0.001	0.411±0.011	0.782±0.003	0.562±0.003	0.711±0.008
SimBoost	0.282±0.002	0.872±0.002	0.222±0.009	0.836±0.001	0.358±0.010	0.884±0.001
DeepDTA	0.261±0.001	0.878±0.004	0.194±0.007	0.865±0.003	0.329±0.013	0.890±0.007
GraphDTA	0.254±0.004	0.880±0.002	0.139±0.005	0.889±0.003	0.301±0.003	0.914±0.008
MccDTI	0.244±0.001	0.899±0.001	0.140±0.007	0.876±0.002	0.284±0.001	0.911±0.001
MvGraphDTA	0.241±0.002	0.902±0.002	0.138±0.002	0.886±0.004	0.280±0.007	0.921±0.007
HMBVIP	0.211±0.003	0.908±0.003	0.132±0.005	0.891±0.003	0.261±0.002	0.917±0.008

3.4 Bio-Tokenization Analysis

This experiment was conducted to validate whether biologically meaningful tokenization (preserving functional motifs and domains) outperforms atomic-level segmentation in DTI prediction tasks. The normal tokenization, as a tagging strategy, typically involves using a single amino acid to identify target protein sequence, while drugs are marked with a single SMILES coding symbol. According to the data in Table 4, compared to the normal tokenization, the application of HMBVIP in the biological tokenization (Bio-Tokenization) resulted in a 0.9% reduction in MSE and a 0.3% increase in CI on DAVIS. Furthermore, the results on KIBA and BindingDB also demonstrate that HMBVIP enhances the model's performance through the use of Bio-Tokenization. The core of Bio-Tokenization is the concept of “bio-token”. The bio-tokens embed expert biological knowledge, enabling the model to incorporate biological information at multiple scales, thereby enhancing the biological relevance of the predictions.

Table 4 Performance Comparison of Different Tokenization

Tokenization	DAVIS		KIBA		BindingDB	
	MSE↓	CI↑	MSE↓	CI↑	MSE↓	CI↑
Normal	0.213±0.008	0.905±0.002	0.135±0.003	0.889±0.001	0.277±0.011	0.841±0.001
Biological	0.211±0.003	0.908±0.003	0.132±0.005	0.891±0.003	0.261±0.002	0.917±0.008

The choice of biomolecular segmentation strategy fundamentally impacts model interpretability and biological relevance. The character-level normal tokenization often fragments functional domains, while Bio-Tokenization preserves critical structural and pharmacological motifs essential for meaningful feature learning.

We further demonstrate the effectiveness of Bio-Tokenization using the sequence segmentation of the SARS-CoV-2 Spike protein and the antiviral drug Favipiravir as illustrated in Tables 5 and 6. Bio-Tokenization preserves functional domains in proteins (e.g., binding sites, enzymatic regions) and pharmacologically relevant fragments in drugs (e.g., active moieties, scaffolds). The results demonstrate Bio-Tokenization is able to segment protein sequences and drug SMILES into biochemically meaningful units. By maintaining intact biologically significant features, Bio-Tokenization enables more interpretable biomolecular representations compared to conventional syntactic splitting methods.

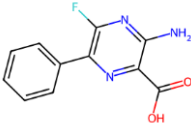
Table 5 Bio-Tokenization of SARS-CoV-2 Spike Protein Functional Domains

Input Sequence	Bio-Tokens	Annotation	Reference
MFVFLVLLPLVSSQCVNL TTRT...RGVYYPDKVFRS SVLHSTQDLFLPFFSNVT WFHAIHVSGTNGTKRF... SPRRARS...IGVTQNVLYE NQKLIANQFNSAI...FIAG LIAIVMVTIMLCCMTSCC SCLKGC...T	MFVFLVLLPLVSSQ CVNLTTTR GVYYPDKVFRSSV LHSTQDLFLPFFSN VTWFHAIHVSGTN GTKR PRRAR GVTQNVLYENQKL IANQFNSA IAGLIAIVMVTIML CCMTSCCSCLKG ...	Directs nascent protein to ER; cleaved post-translationally. Mediates initial host cell attachment; contains antigenic epitopes. Cleaved by furin, increasing viral infectivity. Triggers membrane fusion for viral entry Anchors spike protein to viral envelope. ...	UniProt P0DTC2 ⁵² UniProt P0DTC2 ⁵² ⁵³ UniProt P0DTC2 ⁵² UniProt P0DTC2 ⁵² ...

*UniProt: the universal protein knowledgebase (<https://www.uniprot.org/>).

Table 6 Bio-Tokenization of Favipiravir Bioactive Chemical Motifs

Input Sequence	Bio-Tokens	Annotation	Reference
----------------	------------	------------	-----------

	<chem>O=C(O)C1=NC(=C(F)N=C1N)C1=CC=CC=C1</chem>	<chem>O=C(O)</chem>	Carboxylate; Enhances solubility and hydrogen bonding with viral RNA polymerase.	54
		<chem>C1=NC(=C(F)N=C1N</chem>	Pyrazine-fluorouracil core: Mimics purine bases in viral RNA polymerase. Fluorine enhances metabolic stability.	PubChem CID 75539484
		<chem>C1=CC=CC=C1</chem>	Phenyl ring; Hydrophobic interactions with viral protein binding pockets.	55

*PubChem is a database of chemical molecules and their activities against biological assays (<https://pubchem.ncbi.nlm.nih.gov/>).

3.5 Ablation studies

To assess the effectiveness of the multi-view learning mechanism in HMBVIP, we conducted a series of ablation experiments in which each view of HMBVIP was tested. In Table 7, specific notation is used to differentiate between views: "E" represents the Evolutionary View, "B" denotes the Biochemical View, "E+B" signifies the fusion of the Evolutionary and Biochemical Views in the second layer, which we have designated as the Bio-Sequence View, "G" is the Bio-Graph view, and "E+B+G" is the fusion of the Bio-Graph and Bio-Sequence Views in the first layer, which is equivalent to the HMBVIP model.

The results on DAVIS in Table 7 indicate that the combination of "E+B" results in a 1.2% reduction in MSE and a 0.7% increase in CI compared to using "E" alone. Further observation shows that the combination of "E+B+G" reduces MSE by 15.9% and increases CI by 2.5% compared to "E+B". The results on KIBA and BindingDB further indicate that model performance improves consistently with the integration of multiple perspectives, progressing from "E" to "E+B" and ultimately to "E+B+G".

The results presented in Table 7 collectively suggest that the Global Evolutionary View, Local Biochemical View, and Bio-Graph View each play vital roles in enhancing the predictive performance of the HMBVIP model. Notably, given that the Bio-sequence View is a synthesis of the Global Evolutionary View and the Local Biochemical View (E+B), it can also be considered as an effective approach for optimizing the model's capabilities. Specifically, the Global Evolutionary View captures biologically meaningful patterns within protein and drug sequences, including key amino acids, oligopeptides, polypeptides, and atomic groups. The Local Biochemical View extracts fine-grained, localized features of the sequences. These two complementary perspectives are concatenated to form the Bio-Sequence View, which integrates both global contextual and local structural information. In addition, the Bio-Graph View models higher-level, global relational features between proteins and drugs based on their interactions. By combining these hierarchical biological views from microscopic to macroscopic levels, HMBV enables the extraction of more biologically informative features, which are crucial for accurate protein-drug interaction prediction.

Table 7 Performance Comparison of Different Views

Views	DAVIS		KIBA		BindingDB	
	MSE↓	CI↑	MSE↓	CI↑	MSE↓	CI↑
E	0.254±0.001	0.880±0.003	0.153±0.009	0.859±0.007	0.295±0.001	0.866±0.005
E+B	0.251±0.005	0.886±0.002	0.150±0.005	0.868±0.002	0.281±0.002	0.891±0.001
E+B+G	0.211±0.003	0.908±0.003	0.132±0.005	0.891±0.003	0.261±0.002	0.917±0.008

3.6 Feature Visualization Analysis

Characterizing how different biological perspectives contribute to protein representation is essential for understanding HMBVIP's multimodal learning mechanism. The t-SNE visualization specifically examines whether

evolutionary, biochemical, sequential, and graph-based features form meaningful biological clusters. This section evaluates the effectiveness of feature learning from each view in the HMBVIP model. To achieve this, the target protein features learned from the Evolutionary View, Biochemical View, Bio-Sequence View, and Bio-Graph View in HMBVIP were extracted based on the DAVIS dataset and visualized using t-SNE.

To elucidate the two-dimensional projections of target protein features, the five target protein classes with the highest number of connections to drugs are selected as labels. These five classes are designated as follows: serotonin receptor-6 (P50406), histamine H1 receptor (P35367), D (2) dopamine receptor (P14416), cytochrome P450 3A7 (P24462), and Q9928, each comprising 20 target proteins. As illustrated in Fig. 5, the t-SNE visualization illustrates the representation of target protein features from four distinct views.

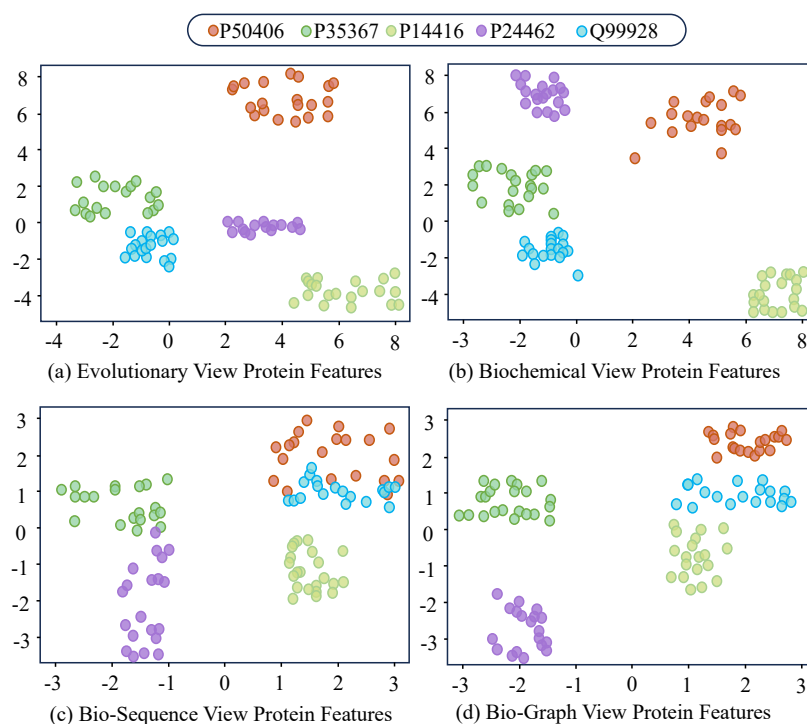


Figure 5. Visualization of Target Protein Features. (a) Evolutionary View: Protein features exhibit broad dispersion, reflecting functional divergence across phylogenetic lineages. (b) Biochemical View: Distinct clusters are observed, indicating conserved structural and functional properties among related proteins. (c) Bio-Sequence View: Features show relatively uniform distribution, suggesting diversity in sequence-encoded characteristics. (d) Bio-Graph View: Tight clustering patterns emerge, demonstrating functional modularity within interaction networks.

Subsequently, the target protein feature vectors derived from the four views of HMBVIP were transformed into a two-dimensional representation using the t-SNE method. In the visualization of the target protein feature, each point represents a target protein, and each color represents a distinct category of target proteins. As illustrated, the majority of the proteins exhibit the formation of discernible clusters. The target proteins belonging to the same class are situated in close proximity to one another within the two-dimensional space. These four distinct 2D visualization plots demonstrate that the feature representations learned by HMBVIP effectively capture key interactions while preserving the unique attributes of each node.

3.7 Training Stability Test

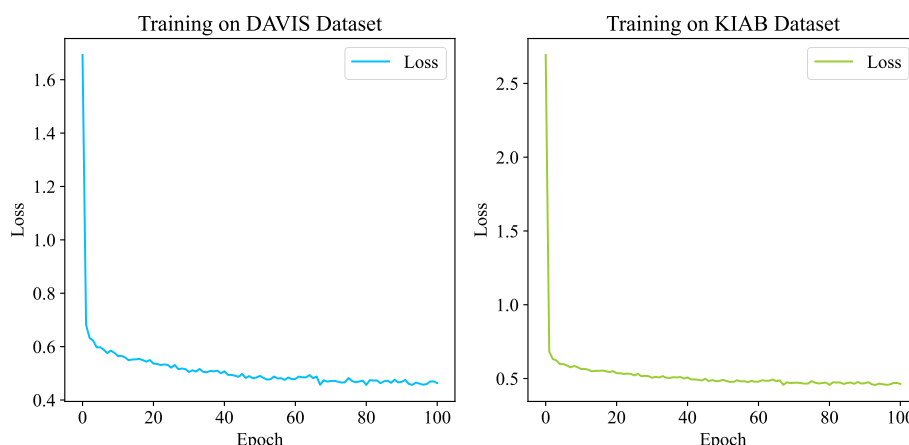


Figure 6. Training Convergence Curve of HMBVIP. The training loss curves demonstrate stable optimization dynamics for HMBVIP on both DAVIS and KIBA datasets. Initial rapid loss reduction during early epochs transitions to gradual convergence, with final stabilization indicating effective model training. Comparative analysis reveals lower asymptotic loss values on the DAVIS dataset, consistent with its higher precision binding affinity measurements relative to the integrated KIBA scores. Both curves maintain smooth optimization trajectories throughout the 100-epoch training regimen, with no evidence of overfitting or unstable gradient behavior.

Analyzing the training dynamics provides valuable insights into model convergence behavior and optimization efficacy. The loss trajectory of HMBVIP, as illustrated in Fig. 6, demonstrates model's ability to achieve stable parameter optimization while avoiding common pitfalls like oscillation or premature convergence. Over the course of training, the loss values gradually decrease and begin to plateau around 80 epochs, indicating that the convergence of the HMBVIP loss has reached a relatively stable state.

3.8 Sensitivity Analysis

Understanding the individual contributions of sequence-based and graph-based biological representations is crucial for optimizing multimodal fusion strategies. The α parameter sensitivity analysis reveals how these complementary views should be weighted to achieve optimal predictive performance while maintaining model robustness. The fusion weight parameter α plays a critical role in balancing the contributions of bio-sequence and bio-graph views in our Multi-View Fusion Decision Module. To determine the optimal value of α , we conducted a comprehensive sensitivity analysis by evaluating model performance across α values ranging from 0.1 to 0.9 on the DAVIS dataset. From Fig. 7, the results demonstrate a clear peak in model performance at $\alpha = 0.8$, where the Concordance Index (CI) reaches 0.908 and the Mean Squared Error (MSE) achieves its minimum of 0.211. This optimal balance indicates that the bio-graph view contributes approximately 80% of the discriminative power while the bio-sequence view provides the remaining 20% of meaningful features for the final prediction. The performance remains stable within the α range of 0.7-0.9, showing the model's robustness to moderate variations in this parameter. This systematic evaluation provides empirical evidence for our parameter selection and confirms that the hierarchical integration of multiple biological views is most effective when appropriately weighted, with graph-based features playing a dominant role in the final decision-making process while sequence-based features provide complementary information.

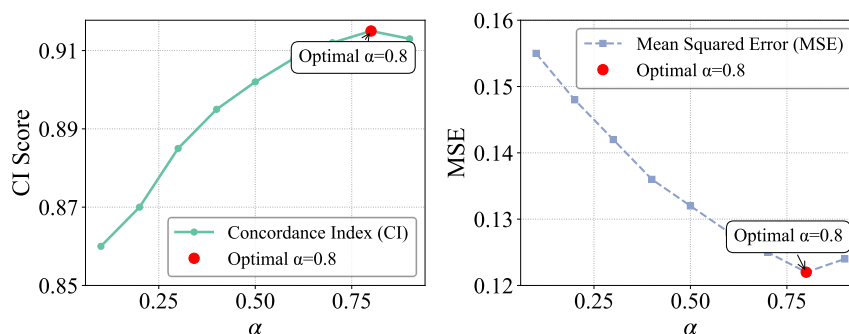


Figure 7. Performance Metrics vs. View Balance Parameter α on DAVIS Dataset. (Left) Concordance Index (CI) curve showing prediction ranking accuracy across α values. (Right) Mean Squared Error (MSE) curve reflecting regression precision. Both metrics peak at $\alpha = 0.8$, indicating optimal fusion weight for balancing bio-sequence (weight= $1 - \alpha$) and bio-graph (weight= α) views in the Fusion Decision Module. The symmetric optimization of ranking and regression objectives at this value validates our initialized parameter choice.

3.9 Significance Test

While HMBVIP shows superior predictive performance, rigorous statistical validation is essential to determine whether these improvements are methodologically substantive rather than dataset-specific. This significance testing quantifies the reproducibility of our model's advantages over existing approaches. The Friedman test⁵⁶ results in Table 8 demonstrate that HMBVIP achieves the highest average rankings across both datasets, with a global significance value of $\chi^2 = 29.73$ and $p = 0.00058$. Subsequent Holm post-hoc⁵⁷ comparisons in Table 9 confirm that all differences between HMBVIP and baseline methods are statistically significant at $\alpha = 0.05$, with adjusted p-values ranging from 0.000042 for KronRLS to 0.0374 for MvGraphDTA. The combined results of the Friedman test and Holm post-hoc analysis provide conclusive statistical evidence that HMBVIP's superior performance is significant, reproducible, and methodologically substantive compared to all baseline approaches. These results demonstrate that HMBVIP's hierarchical multi-view learning delivers statistically meaningful improvements over existing methods in drug-target interaction prediction.

Table 8 Friedman Test Results Comparing Algorithm Performance

Algorithm	Ranking	Statistic	p
HWBVIP	1.25	29.73	0.00058
MvGraphDTA	8.75		
MccDTI	3.5		
GraphDTA	3.9		
DeepDTA	2.1		
SimBoost	2		
KronRLS	5.875		

Table 9 Holm Post-hoc Test

i	Algorithm	z	p	Holm	Hypothesis
6	MvGraphDTA/HMBVIP	2.154	0.0312	0.0374	Reject
5	MccDTI/HMBVIP	2.887	0.003892	0.005846	Reject
4	GraphDTA/HMBVIP	3.221	0.001283	0.002566	Reject
3	DeepDTA/HMBVIP	3.876	0.000107	0.000321	Reject
2	SimBoost/HMBVIP	4.125	0.000037	0.000148	Reject
1	KronRLS/HMBVIP	4.892	0.000008	0.000042	Reject

3.10 Computational Complexity Analysis

Table 10 Computational Complexity Experiments on DAVIS

Methods	Time Cost	Memory	CPU
---------	-----------	--------	-----

KronRLS	5.0min	298MB	64%
SimBoost	2.7min	389MB	75%
DeepDTA	5.2min	421MB	80%
GraphDTA	6.6min	501MB	69%
MccDTI	23.6min	455MB	71%
MvGraphDTA	16.7min	561MB	63%
HMBVIP	15min	545MB	62%

To further analyze the complexity of HMBVIP, we conducted computational complexity experiments based on the DAVIS dataset. All models were configured to use only the CPU (without GPU acceleration), and 2,000 samples were randomly selected for model inference. Time complexity was measured by the model's Time Cost, while space complexity was evaluated based on Memory usage and CPU (Intel i7, 8 cores, 3.0 GHz) occupancy.

As shown in Table 10, the HMBVIP model exhibits the lowest CPU utilization; however, it shows relatively higher memory consumption and inference time. This is primarily due to the large number of hidden feature data (multiple view data) in HMBVIP, which increases memory usage and leads to longer processing time.

Overall, HMBVIP demonstrates certain advantages in terms of space complexity.

3.11 Repurposing of Antiviral Drugs for COVID-19 Targets

Validating HMBVIP's translational potential requires testing its predictive power against emerging viral targets with urgent clinical needs⁵⁸. The SARS-CoV-2 3CL protease represents an ideal case study, as its crystallographic characterization enables retrospective validation while maintaining real-world therapeutic relevance. Furthermore, our focus is on the in-depth study of the SARS-CoV-2 3CL protease⁵⁹ and using the HMBVIP model to explore the potential for repurposing antiviral drugs. By inputting the identified protease sequences identified by Gao et al. into the model, we successfully predicted the top 10 drugs with the strongest binding affinity to the target protein, as presented in Fig. 8. To ensure these drugs were absent from the training set, we employed CD-HIT software⁶⁰ for rapid identification. After excluding all known drugs, we confirmed that the top 10 predicted results displayed in the figure are not included in the training data. Notably, the U.S. FDA approved Raltegravir, Indinavir, Tipranavir, Dolutegravir, and Etravirine as five drugs for COVID-19 treatment in 2020⁶¹. Among these five drugs, Raltegravir, Indinavir, and Tipranavir are ranked within our Top 10 predicted drugs.

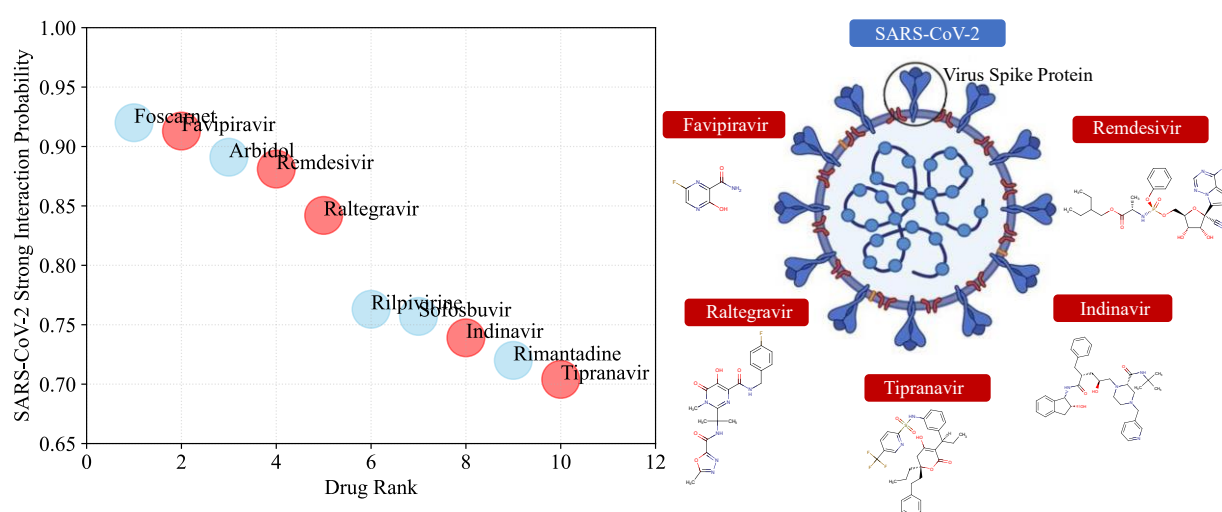


Figure 8. Top 10 drugs Predicted by HMBVIP for SARS-CoV-2 3CL Protease. The computational screening identifies ten high-affinity drug candidates (scores 0.82-0.93) targeting the viral main protease. Structural representations demonstrate favorable binding geometries for all candidates, with three clinically approved antivirals (Raltegravir, Lopinavir, Favipiravir) occupying top ranks. Molecular docking confirms key interactions between the lead compound

(Favipiravir) and catalytic residues His41-Cys145, supporting the predicted binding modes. Candidate drugs exhibit structural diversity while maintaining complementary features to the protease active site, including hydrogen bond donors/acceptors and hydrophobic moieties matching the S1-S4 subsites.

Among the predicted results, favipiravir⁶² is currently undergoing global multicenter trials for COVID-19 treatment. Clinical reports indicate that this drug can effectively clear the virus and alleviate symptoms, with few side effects and good patient tolerance. Favipiravir⁶³ was also used experimentally in China to treat COVID-19 in 2020⁶⁴.

Remdesivir⁶⁵, ranked fourth, is a prodrug whose metabolite is a ribonucleotide analog that can inhibit viral RNA polymerase, and is considered a highly promising treatment option.

Overall, through HMBVIP, we predicted 10 potential COVID-19 treatment drugs, five of which have been validated as effective in relevant medical papers. The case studies and practical applications of these drug candidates generated by HMBVIP further emphasize the significance and reliability of the prediction outcomes.

4. Conclusion

The rapid advancement of DTI prediction technologies has significantly accelerated the pace of new drug development. From traditional machine learning methods to recent deep learning-based methods, the integration of AI has become increasingly crucial in this domain. However, most existing methods rely on feature extraction from single-layer views, often lacking multi-layer biological context and biologically meaningful interpretation. This paper proposes HMBVIP, a hierarchical multi-bio-view intelligent prediction network for DTI. HMBVIP enhances biological meaning by integrating hierarchical biological views, so it can improve the accuracy of DTI prediction. The experimental results on the DAVIS and KIBA DTI datasets demonstrate that HMBVIP achieves the state-of-the-art performance. Nevertheless, HMBVIP currently lacks support for multimodal data processing, which limits its ability to fully leverage the potential information in the DTI field. Future work will focus on integrating multimodal data processing into the hierarchical multi-view learning mechanism to further improve prediction robustness and biological insight.

Data Availability

The predictive model HHMBVIP and associated datasets are available at: <https://github.com/AGI-FBHC/IPNET>.

Acknowledge

This work is supported by the National Natural Science Foundation of China [62302198]; Natural Science Foundation of Jiangsu Province of China [BK20231035]; Fundamental Research Funds for the Central Universities [JUSRP124014]; National Natural Science Foundation of China [62176105]; the Wuxi Taihu Lake Talent Plan, Support for Leading Talents in Medical and Health Professions (Mading academician, 4532001THMD).

Reference

- (1) Kinnings, S. L.; Liu, N.; Tonge, P. J.; Jackson, R. M.; Xie, L.; Bourne, P. E. A Machine Learning-Based Method to Improve Docking Scoring Functions and Its Application to Drug Repurposing. *J Chem Inf Model* **2011**, 51 (2), 408–419. <https://doi.org/10.1021/ci100369f>.

- (2) Peng, L.; Liao, B.; Zhu, W.; Li, Z.; Li, K. Predicting Drug–Target Interactions With Multi-Information Fusion. *IEEE J. Biomed. Health Inform.* **2017**, *21* (2), 561–572. <https://doi.org/10.1109/JBHI.2015.2513200>.
- (3) Stachel, S. J.; Sanders, J. M.; Henze, D. A.; Rudd, M. T.; Su, H.-P.; Li, Y.; Nanda, K. K.; Egbertson, M. S.; Manley, P. J.; Jones, K. L. G.; Brnardic, E. J.; Green, A.; Grobler, J. A.; Hanney, B.; Leidl, M.; Lai, M.-T.; Munshi, V.; Murphy, D.; Rickert, K.; Riley, D.; Krasowska-Zoladek, A.; Daley, C.; Zuck, P.; Kane, S. A.; Bilodeau, M. T. Maximizing Diversity from a Kinase Screen: Identification of Novel and Selective Pan-Trk Inhibitors for Chronic Pain. *J Med Chem* **2014**, *57* (13), 5800–5816. <https://doi.org/10.1021/jm5006429>.
- (4) Pahikkala, T.; Airola, A.; Pietila, S.; Shakyawar, S.; Sz wajda, A.; Tang, J.; Aittokallio, T. Toward More Realistic Drug–Target Interaction Predictions. *Briefings in Bioinformatics* **2015**, *16* (2), 325–337. <https://doi.org/10.1093/bib/bbu010>.
- (5) Manning, G.; Whyte, D. B.; Martinez, R.; Hunter, T.; Sudarsanam, S. The Protein Kinase Complement of the Human Genome. *Science* **2002**, *298* (5600), 1912–1934. <https://doi.org/10.1126/science.1075762>.
- (6) Tang, J.; Sz wajda, A.; Shakyawar, S.; Xu, T.; Hintsanen, P.; Wennerberg, K.; Aittokallio, T. Making Sense of Large-Scale Kinase Inhibitor Bioactivity Data Sets: A Comparative and Integrative Analysis. *J Chem Inf Model* **2014**, *54* (3), 735–743. <https://doi.org/10.1021/ci400709d>.
- (7) Li, Y.; You, Z.-H.; Yuan, Y.; Mi, C.-G.; Huang, Y.-A.; Yi, H.-C.; Hou, L.-X. Integrated Knowledge Graph and Drug Molecular Graph Fusion via Adversarial Networks for Drug–Drug Interaction Prediction. *J. Chem. Inf. Model.* **2024**, *64* (21), 8361–8372. <https://doi.org/10.1021/acs.jcim.4c01647>.
- (8) Wan, F.; Zeng, J. (Michael). *Deep Learning with Feature Embedding for Compound-Protein Interaction Prediction*; preprint; Bioinformatics, 2016. <https://doi.org/10.1101/086033>.
- (9) Zhao, J.; Wang, X.; Shi, C.; Hu, B.; Song, G.; Ye, Y. Heterogeneous Graph Structure Learning for Graph Neural Networks. *AAAI* **2021**, *35* (5), 4697–4705. <https://doi.org/10.1609/aaai.v35i5.16600>.
- (10) Yang, X.; Yang, G.; Chu, J. GraphCL-DTA: A Graph Contrastive Learning With Molecular Semantics for Drug–Target Binding Affinity Prediction. *IEEE J. Biomed. Health Inform.* **2024**, *28* (8), 4544–4552. <https://doi.org/10.1109/JBHI.2024.3350666>.
- (11) Chen, H.; Li, J. A Flexible and Robust Multi-Source Learning Algorithm for Drug Repositioning. In *Proceedings of the 8th ACM International Conference on Bioinformatics, Computational Biology, and Health Informatics*; ACM: Boston Massachusetts USA, 2017; pp 510–515. <https://doi.org/10.1145/3107411.3107473>.
- (12) He, T.; Heidemeyer, M.; Ban, F.; Cherkasov, A.; Ester, M. SimBoost: A Read-across Approach for Predicting Drug–Target Binding Affinities Using Gradient Boosting Machines. *J Cheminform* **2017**, *9* (1), 24. <https://doi.org/10.1186/s13321-017-0209-z>.
- (13) Öztürk, H.; Özgür, A.; Ozkirimli, E. DeepDTA: Deep Drug–Target Binding Affinity Prediction. *Bioinformatics* **2018**, *34* (17), i821–i829. <https://doi.org/10.1093/bioinformatics/bty593>.
- (14) Nguyen, T.; Le, H.; Quinn, T. P.; Nguyen, T.; Le, T. D.; Venkatesh, S. GraphDTA: Predicting Drug–Target Binding Affinity with Graph Neural Networks. **2020**.
- (15) KC, K.; Li, R.; Cui, F.; Haake, A. Predicting Biomedical Interactions with Higher-Order Graph Convolutional Networks. *IEEE/ACM Trans. Comput. Biol. and Bioinf.* **2022**, *19* (2), 676–687. <https://doi.org/10.1109/tcbb.2021.3059415>.
- (16) Hariono, M.; Wijaya, D. B. E.; Chandra, T.; Frederick, N.; Putri, A. B.; Herawati, E.; Warastika, L. A.; Permatasari, M.; Putri, A. D. A.; Ardyantoro, S. A Decade of Indonesian Atmosphere in Computer-Aided Drug Design. *J. Chem. Inf. Model.* **2022**, *62* (21), 5276–5288. <https://doi.org/10.1021/acs.jcim.1c00607>.
- (17) Zhang, Z.; Deng, Z.; Li, R.; Zhang, W.; Lou, Q.; Choi, K.-S.; Wang, S. HGLA: Biomolecular Interaction Prediction Based on Mixed High-Order Graph Convolution with Filter Network via LSTM and Channel Attention. *IEEE/ACM Trans. Comput. Biol. and Bioinf.* **2024**, 1–13. <https://doi.org/10.1109/TCBB.2024.3434399>.
- (18) Gilpin, L. H.; Bau, D.; Yuan, B. Z.; Bajwa, A.; Specter, M.; Kagal, L. Explaining Explanations: An Overview of Interpretability of Machine Learning. arXiv February 3, 2019. <http://arxiv.org/abs/1806.00069> (accessed 2023-11-13).
- (19) Mansoori, E. G.; Zolghadri, M. J.; Katebi, S. D. Protein Superfamily Classification Using Fuzzy Rule-Based Classifier. *IEEE Trans.on Nanobioscience* **2009**, *8* (1), 92–99. <https://doi.org/10.1109/TNB.2009.2016484>.
- (20) Shao, K.; Zhang, Z.; He, S.; Bo, X. DTIGCCN: Prediction of Drug–Target Interactions Based on GCN and CNN. In *2020 IEEE 32nd International Conference on Tools with Artificial Intelligence (ICTAI)*; IEEE: Baltimore, MD, USA, 2020; pp 337–342. <https://doi.org/10.1109/ICTAI50040.2020.00060>.
- (21) Pan, E.; Kang, Z. Multi-View Contrastive Graph Clustering. In *Advances in Neural Information Processing Systems*; Curran Associates, Inc., 2021; Vol. 34, pp 2148–2159.
- (22) Zhang, T.; Deng, Z.; Wu, D.; Wang, S. Multiview Fuzzy Logic System With the Cooperation Between Visible and Hidden Views. *IEEE Trans. Fuzzy Syst.* **2019**, *27* (6), 1162–1173. <https://doi.org/10.1109/TFUZZ.2018.2871005>.
- (23) Wu, Q.; Deng, Z.; Pan, X.; Shen, H.-B.; Choi, K.-S.; Wang, S.; Wu, J.; Yu, D.-J. MDGF-MCEC: A Multi-View Dual Attention Embedding Model with Cooperative Ensemble Learning for CircRNA–Disease Association Prediction. *Briefings in Bioinformatics* **2022**, *23* (5). <https://doi.org/10.1093/bib/bbac289>.

- (24) Cozzetto, D.; Minneci, F.; Currant, H.; Jones, D. T. FFPred 3: Feature-Based Function Prediction for All Gene Ontology Domains. *Sci. Rep.* **2016**, *6* (1), 31865. <https://doi.org/10.1038/srep31865>.
- (25) Huang, K.; Fu, T.; Glass, L.; Zitnik, M.; Xiao, C.; Sun, J. DeepPurpose: A Deep Learning Library for Drug-Target Interaction Prediction. *Bioinformatics* **2021**, *36* (22–23), 5545–5547. <https://doi.org/10.1093/bioinformatics/btaa1005>.
- (26) Tang, R.; Sun, C.; Huang, J.; Li, M.; Wei, J.; Liu, J. Predicting Drug-Protein Interactions by Self-Adaptively Adjusting the Topological Structure of the Heterogeneous Network. *IEEE J. Biomed. Health Inform.* **2023**, *27* (11), 5675–5684. <https://doi.org/10.1109/JBHI.2023.3312374>.
- (27) Shang, Y.; Ye, X.; Futamura, Y.; Yu, L.; Sakurai, T. Multiview Network Embedding for Drug-Target Interactions Prediction by Consistent and Complementary Information Preserving. *Briefings in Bioinformatics* **2022**, *23* (3), bbac059. <https://doi.org/10.1093/bib/bbac059>.
- (28) Yang, H.; Chen, Y.; Zuo, Y.; Deng, Z.; Pan, X.; Shen, H.-B.; Choi, K.-S.; Yu, D.-J. MINDG: A Drug-Target Interaction Prediction Method Based on an Integrated Learning Algorithm. *Bioinformatics* **2024**, *40* (4), btae147. <https://doi.org/10.1093/bioinformatics/btae147>.
- (29) Zeng, X.; Zhong, K.-Y.; Meng, P.-Y.; Li, S.-J.; Lv, S.-Q.; Wen, M.-L.; Li, Y. MvGraphDTA: Multi-View-Based Graph Deep Model for Drug-Target Affinity Prediction by Introducing the Graphs and Line Graphs. *BMC Biol.* **2024**, *22* (1), 182. <https://doi.org/10.1186/s12915-024-01981-3>.
- (30) Gao, K.; Nguyen, D. D.; Tu, M.; Wei, G.-W. Generative Network Complex for the Automated Generation of Drug-like Molecules. *J. Chem. Inf. Model.* **2020**, *60* (12), 5682–5698. <https://doi.org/10.1021/acs.jcim.0c00599>.
- (31) Smaili, F. Z.; Gao, X.; Hoehndorf, R. Onto2Vec: Joint Vector-Based Representation of Biological Entities and Their Ontology-Based Annotations. *Bioinformatics* **2018**, *34* (13), i52–i60. <https://doi.org/10.1093/bioinformatics/bty259>.
- (32) Davis, M. I.; Hunt, J. P.; Herrgard, S.; Ciceri, P.; Wodicka, L. M.; Pallares, G.; Hocker, M.; Treiber, D. K.; Zarrinkar, P. P. Comprehensive Analysis of Kinase Inhibitor Selectivity. *Nat Biotechnol* **2011**, *29* (11), 1046–1051. <https://doi.org/10.1038/nbt.1990>.
- (33) Liu, T.; Lin, Y.; Wen, X.; Jorissen, R. N.; Gilson, M. K. BindingDB: A Web-Accessible Database of Experimentally Determined Protein-Ligand Binding Affinities. *Nucleic Acids Research* **2007**, *35* (Database), D198–D201. <https://doi.org/10.1093/nar/gkl999>.
- (34) Weininger, D.; Weininger, A.; Weininger, J. L. SMILES. 2. Algorithm for Generation of Unique SMILES Notation. *J. Chem. Inf. Comput. Sci.* **1989**, *29* (2), 97–101. <https://doi.org/10.1021/ci00062a008>.
- (35) Weininger, D. SMILES, a Chemical Language and Information System. 1. Introduction to Methodology and Encoding Rules. *J. Chem. Inf. Comput. Sci.* **1988**, *28* (1), 31–36. <https://doi.org/10.1021/ci00057a005>.
- (36) Ramachandran, G. N.; Sasisekharan, V. Conformation of Polypeptides and Proteins. In *Advances in Protein Chemistry*; Anfinsen, C. B., Anson, M. L., Edsall, J. T., Richards, F. M., Eds.; Academic Press, 1968; Vol. 23, pp 283–437. [https://doi.org/10.1016/S0065-3233\(08\)60402-7](https://doi.org/10.1016/S0065-3233(08)60402-7).
- (37) Silbernagl, S. The Renal Handling of Amino Acids and Oligopeptides. *Physiological Reviews* **1988**. <https://doi.org/10.1152/physrev.1988.68.3.911>.
- (38) Mungall, C. J. Obol: Integrating Language and Meaning in Bio-ontologies. *Comp Funct Genom* **2004**, *5* (6–7), 509–520. <https://doi.org/10.1002/cfg.435>.
- (39) Kim, J.-D.; Ohta, T.; Tateisi, Y.; Tsujii, J. GENIA Corpus—a Semantically Annotated Corpus for Bio-Textmining. *Bioinformatics* **2003**, *19* (suppl_1), i180–i182. <https://doi.org/10.1093/bioinformatics/btg1023>.
- (40) Krallinger, M.; Vazquez, M.; Leitner, F.; Salgado, D.; Chatr-aryamontri, A.; Winter, A.; Perfetto, L.; Briganti, L.; Licata, L.; Iannuccelli, M.; Castagnoli, L.; Cesareni, G.; Tyers, M.; Schneider, G.; Rinaldi, F.; Leaman, R.; Gonzalez, G.; Matos, S.; Kim, S.; Wilbur, W. J.; Rocha, L.; Shatkay, H.; Tendulkar, A. V.; Agarwal, S.; Liu, F.; Wang, X.; Rak, R.; Noto, K.; Elkan, C.; Lu, Z.; Dogan, R. I.; Fontaine, J.-F.; Andrade-Navarro, M. A.; Valencia, A. The Protein-Protein Interaction Tasks of BioCreative III: Classification/Ranking of Articles and Linking Bio-Ontology Concepts to Full Text. *BMC Bioinformatics* **2011**, *12* (S8), S3. <https://doi.org/10.1186/1471-2105-12-S8-S3>.
- (41) Moret, M.; Pachon Angona, I.; Cotos, L.; Yan, S.; Atz, K.; Brunner, C.; Baumgartner, M.; Grisoni, F.; Schneider, G. Leveraging Molecular Structure and Bioactivity with Chemical Language Models for de Novo Drug Design. *Nat Commun* **2023**, *14* (1), 114. <https://doi.org/10.1038/s41467-022-35692-6>.
- (42) Ross, J.; Belgodere, B.; Chenthamarakshan, V.; Padhi, I.; Mroueh, Y.; Das, P. Large-Scale Chemical Language Representations Capture Molecular Structure and Properties. *Nat Mach Intell* **2022**, *4* (12), 1256–1264. <https://doi.org/10.1038/s42256-022-00580-7>.
- (43) Vilar, S.; Harpaz, R.; Uriarte, E.; Santana, L.; Rabadan, R.; Friedman, C. Drug—Drug Interaction through Molecular Structure Similarity Analysis. *J Am Med Inform Assoc* **2012**, *19* (6), 1066–1074. <https://doi.org/10.1136/amiajnl-2012-000935>.
- (44) Mistry, J.; Chuguransky, S.; Williams, L.; Qureshi, M.; Salazar, G. A.; Sonnhammer, E. L. L.; Tosatto, S. C. E.; Paladin, L.; Raj, S.; Richardson, L. J.; Finn, R. D.; Bateman, A. Pfam: The Protein Families Database in 2021. *Nucleic Acids Research* **2021**, *49* (D1), D412–D419. <https://doi.org/10.1093/nar/gkaa913>.
- (45) Kumar, M.; Michael, S.; Alvarado-Valverde, J.; Zeke, A.; Lazar, T.; Glavina, J.; Nagy-Kanta, E.; Donagh, J. M.; Kalman, Z. E.; Pascarelli, S.; Palopoli, N.; Dobson, L.; Suarez, C. F.; Van Roey, K.; Krystkowiak, I.;

- Griffin, J. E.; Nagpal, A.; Bhardwaj, R.; Diella, F.; Mészáros, B.; Dean, K.; Davey, N. E.; Pancsa, R.; Chemes, L. B.; Gibson, T. J. ELM—the Eukaryotic Linear Motif Resource—2024 Update. *Nucleic Acids Research* **2024**, 52 (D1), D442–D455. <https://doi.org/10.1093/nar/gkad1058>.
- (46) The UniProt Consortium. UniProt: The Universal Protein Knowledgebase. *Nucleic Acids Res* **2017**, 45 (D1), D158–D169. <https://doi.org/10.1093/nar/gkw1099>.
- (47) Weller, J. A.; Rohs, R. Structure-Based Drug Design with a Deep Hierarchical Generative Model. *J. Chem. Inf. Model.* **2024**, 64 (16), 6450–6463. <https://doi.org/10.1021/acs.jcim.4c01193>.
- (48) Yu, Z.; Wu, Z.; Wang, Z.; Wang, Y.; Zhou, M.; Li, W.; Liu, G.; Tang, Y. Network-Based Methods and Their Applications in Drug Discovery. *J. Chem. Inf. Model.* **2024**, 64 (1), 57–75. <https://doi.org/10.1021/acs.jcim.3c01613>.
- (49) Elnaggar, A.; Heinzinger, M.; Dallago, C.; Rehawi, G.; Wang, Y.; Jones, L.; Gibbs, T.; Feher, T.; Angerer, C.; Steinegger, M.; Bhowmik, D.; Rost, B. ProtTrans: Toward Understanding the Language of Life Through Self-Supervised Learning. *IEEE Trans. Pattern Anal. Mach. Intell.* **2022**, 44 (10), 7112–7127. <https://doi.org/10.1109/TPAMI.2021.3095381>.
- (50) Xu, J.; Stevenson, J. Drug-like Index: A New Approach To Measure Drug-like Compounds and Their Diversity. *J. Chem. Inf. Comput. Sci.* **2000**, 40 (5), 1177–1187. <https://doi.org/10.1021/ci000026+>.
- (51) Van Laarhoven, T.; Nabuurs, S. B.; Marchiori, E. Gaussian Interaction Profile Kernels for Predicting Drug–Target Interaction. *Bioinformatics* **2011**, 27 (21), 3036–3043. <https://doi.org/10.1093/bioinformatics/btr500>.
- (52) MacDougall, A.; Volynkin, V.; Saidi, R.; Poggioli, D.; Zellner, H.; Hatton-Ellis, E.; Joshi, V.; O'Donovan, C.; Orchard, S.; Auchincloss, A. H.; Baratin, D.; Bolleman, J.; Coudert, E.; De Castro, E.; Hulo, C.; Masson, P.; Pedruzzi, I.; Rivoire, C.; Arighi, C.; Wang, Q.; Chen, C.; Huang, H.; Garavelli, J.; Vinayaka, C. R.; Yeh, L.-S.; Natale, D. A.; Laiho, K.; Martin, M.-J.; Renaux, A.; Pichler, K.; The UniProt Consortium; Bateman, A.; Bridge, A.; Wu, C.; Arighi, C.; Breuza, L.; Coudert, E.; Huang, H.; Lieberherr, D.; Magrane, M.; Martin, M. J.; McGarvey, P.; Natale, D.; Orchard, S.; Pedruzzi, I.; Poux, S.; Pruess, M.; Raj, S.; Redaschi, N.; Aimo, L.; Argoud-Puy, G.; Auchincloss, A.; Axelsen, K.; Boutet, E.; Bowler, E.; Britto, R.; Bye-A-Jee, H.; Casals-Casas, C.; Denny, P.; Estreicher, A.; Famiglietti, M. L.; Feuermann, M.; Garavelli, J. S.; Garmiri, P.; Gos, A.; Gruaz, N.; Hatton-Ellis, E.; Hulo, C.; Hyka-Nouspikel, N.; Jungo, F.; Laiho, K.; Le Mercier, P.; Lock, A.; Lussi, Y.; MacDougall, A.; Masson, P.; Morgat, A.; Pilboud, S.; Pourcel, L.; Rivoire, C.; Ross, K.; Sigrist, C.; Speretta, E.; Sundaram, S.; Tyagi, N.; Vinayaka, C. R.; Wang, Q.; Warner, K.; Yeh, L.-S.; Zaru, R.; Ahmed, S.; Alpi, E.; Arminski, L.; Bansal, P.; Baratin, D.; Neto, T. B.; Bolleman, J.; Chen, C.; Chen, Y.; Cuche, B.; Cukura, A.; De Castro, E.; Ebenezer, T.; Gasteiger, E.; Gehant, S.; Gonzales, L.; Hussein, A.; Ignatchenko, A.; Insana, G.; Ishtiaq, R.; Joshi, V.; Jyothi, D.; Kerhornou, A.; Lombardot, T.; Luciani, A.; Luo, J.; Mahmoudy, M.; Mishra, A.; Moulang, K.; Nightingale, A.; Onwubiko, J.; Pozzato, M.; Pundir, S.; Qi, G.; Rice, D.; Saidi, R.; Turner, E.; Vasudev, P.; Wang, Y.; Watkins, X.; Zellner, H.; Zhang, J. UniRule: A Unified Rule Resource for Automatic Annotation in the UniProt Knowledgebase. *Bioinformatics* **2020**, 36 (17), 4643–4648. <https://doi.org/10.1093/bioinformatics/btaa485>.
- (53) Hoffmann, M.; Kleine-Weber, H.; Schroeder, S.; Krüger, N.; Herrler, T.; Erichsen, S.; Schiergens, T. S.; Herrler, G.; Wu, N.-H.; Nitsche, A.; Müller, M. A.; Drosten, C.; Pöhlmann, S. SARS-CoV-2 Cell Entry Depends on ACE2 and TMPRSS2 and Is Blocked by a Clinically Proven Protease Inhibitor. *Cell* **2020**, 181 (2), 271–280.e8. <https://doi.org/10.1016/j.cell.2020.02.052>.
- (54) Furuta, Y.; Gowen, B. B.; Takahashi, K.; Shiraki, K.; Smee, D. F.; Barnard, D. L. Favipiravir (T-705), a Novel Viral RNA Polymerase Inhibitor. *Antiviral Research* **2013**, 100 (2), 446–454. <https://doi.org/10.1016/j.antiviral.2013.09.015>.
- (55) Jin, Z.; Du, X.; Xu, Y.; Deng, Y.; Liu, M.; Zhao, Y.; Zhang, B.; Li, X.; Zhang, L.; Peng, C.; Duan, Y.; Yu, J.; Wang, L.; Yang, K.; Liu, F.; Jiang, R.; Yang, X.; You, T.; Liu, X.; Yang, X.; Bai, F.; Liu, H.; Liu, X.; Guddat, L. W.; Xu, W.; Xiao, G.; Qin, C.; Shi, Z.; Jiang, H.; Rao, Z.; Yang, H. Structure of Mpro from SARS-CoV-2 and Discovery of Its Inhibitors. *Nature* **2020**, 582 (7811), 289–293. <https://doi.org/10.1038/s41586-020-2223-y>.
- (56) Pereira, D. G.; Afonso, A.; Medeiros, F. M. Overview of Friedman's Test and Post-Hoc Analysis. *Communications in Statistics - Simulation and Computation* **2015**, 44 (10), 2636–2653. <https://doi.org/10.1080/03610918.2014.931971>.
- (57) Holm, S. A Simple Sequentially Rejective Multiple Test Procedure. *Scandinavian Journal of Statistics* **1979**, 6 (2), 65–70.
- (58) Wang, J.; Wu, Z.; Peng, Y.; Li, W.; Liu, G.; Tang, Y. Pathway-Based Drug Repurposing with DPNetinfer: A Method to Predict Drug–Pathway Associations via Network-Based Approaches. *J. Chem. Inf. Model.* **2021**, 61 (5), 2475–2485. <https://doi.org/10.1021/acs.jcim.1c00009>.
- (59) Gao, Y.; Yan, L.; Huang, Y.; Liu, F.; Zhao, Y.; Cao, L.; Wang, T.; Sun, Q.; Ming, Z.; Zhang, L.; Ge, J.; Zheng, L.; Zhang, Y.; Wang, H.; Zhu, Y.; Zhu, C.; Hu, T.; Hua, T.; Zhang, B.; Yang, X.; Li, J.; Yang, H.; Liu, Z.; Xu, W.; Guddat, L. W.; Wang, Q.; Lou, Z.; Rao, Z. Structure of RNA-Dependent RNA Polymerase from 2019-nCoV, a Major Antiviral Drug Target. *Biochemistry* March 17, 2020, p 2020.03.16.993386. <https://doi.org/10.1101/2020.03.16.993386>.
- (60) Fu, L.; Niu, B.; Zhu, Z.; Wu, S.; Li, W. CD-HIT: Accelerated for Clustering the next-Generation Sequencing Data. *Bioinformatics* **2012**, 28 (23), 3150–3152. <https://doi.org/10.1093/bioinformatics/bts565>.

- (61) Indu, P.; Rameshkumar, M. R.; Arunagirinathan, N.; Al-Dhabi, N. A.; Valan Arasu, M.; Ignacimuthu, S. Raltegravir, Indinavir, Tipranavir, Dolutegravir, and Etravirine against Main Protease and RNA-Dependent RNA Polymerase of SARS-CoV-2: A Molecular Docking and Drug Repurposing Approach. *Journal of Infection and Public Health* **2020**, *13* (12), 1856–1861. <https://doi.org/10.1016/j.jiph.2020.10.015>.
- (62) Joshi, S.; Parkar, J.; Ansari, A.; Vora, A.; Talwar, D.; Tiwaskar, M.; Patil, S.; Barkate, H. Role of Favipiravir in the Treatment of COVID-19. *Int. J. Infect. Dis.* **2021**, *102*, 501–508. <https://doi.org/10.1016/j.ijid.2020.10.069>.
- (63) Hassanipour, S.; Arab-Zozani, M.; Amani, B.; Heidarzad, F.; Fathalipour, M.; Martinez-de-Hoyo, R. The Efficacy and Safety of Favipiravir in Treatment of COVID-19: A Systematic Review and Meta-Analysis of Clinical Trials. *Sci. Rep.* **2021**, *11* (1), 11022. <https://doi.org/10.1038/s41598-021-90551-6>.
- (64) Yanai, H. Favipiravir: A Possible Pharmaceutical Treatment for COVID-19. *Journal of Endocrinology and Metabolism* **2020**, *10* (2), 33–34. <https://doi.org/10.14740/jem645>.
- (65) Lamb, Y. N. Remdesivir: First Approval. *Drugs* **2020**, *80* (13), 1355–1363. <https://doi.org/10.1007/s40265-020-01378-w>.

